Research Article

Effect of SiO_2 nanoparticle addition on growth of interfacial Ag_3Sn intermetallic compound layers between lead-free solder and silver conductor

Hsing-I Hsiang[1] · Chih-Cheng Chen[2] · Han-Yang Su[1]

Received: 20 July 2021 / Accepted: 2 November 2021
Published online: 14 November 2021

© The Author(s) 2021 OPEN

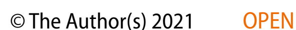

Abstract
This study investigated the effects of silver powder modification on intermetallic compound (IMC) formation and silver leaching during soldering at high temperatures. Silica nanoparticles (NPs) were deposited onto a silver powder surface to inhibit silver leaching, which can lead to soldering joint failure during high-temperature soldering. The NPs were deposited through hydrolysis and a condensation reaction of tetraethyl orthosilicate (TEOS) based on the Stöber method. Fourier transform infrared spectroscopy and scanning electron microscopy were used to observe the microstructures of silver powders after the deposition of silica NPs with various TEOS concentrations and various deposition times. As the deposition time increased, the amount of silica NPs on the surface of the silver powder increased. The transmission electron microscopy results show that silica NPs were located at the IMC grain boundaries, which can hinder the dissolution of IMCs by lead-free solder melt along grain boundaries during soldering, retarding silver leaching. The growth kinetics and mechanism of IMCs during soldering were investigated. The results show that the growth of IMCs is mainly dominated by bulk diffusion. The activation energy for IMC growth increased and the growth rate decreased with increasing silica NP addition and deposition time.

Keywords Lead-free solder · Silver paste · Ag_3Sn · Intermetallic compound · Silica nanoparticle

1 Introduction

Lead-free solder, which is widely used in the electronics industry to meet the Restriction of Hazardous Substances (RoHS) Directive requirements, often requires a soldering temperature of higher than 270 °C. Conductor loss contributes significantly to the total loss for microwave devices. Silver-based conductors are widely used in microwave devices for consumer wireless packaging applications due to their excellent conductivity. However, silver conductors formed using Ag paste consist of only Ag metal powder, which has a low resistance to solder leaching [1]. During soldering at temperatures above 200 °C, a two-phase equilibrium between the intermetallic compound (IMC) Ag_3Sn and a tin-rich liquid is reached. The tin-rich liquid phase dissolves Ag [2]. Therefore, silver leaching (typically the dissolution of silver in a conductor pattern into the solder) easily occurs at high soldering temperatures. Because the Ag_3Sn phase that forms in the solder due to silver leaching is rigid and brittle, cracks easily occur along

Supplementary Information The online version contains supplementary material available at https://doi.org/10.1007/s42452-021-04861-5.

✉ Hsing-I Hsiang, hsingi@mail.ncku.edu.tw | [1]Department of Resources Engineering, National Cheng Kung University, Tainan, Taiwan. [2]Department of Mechanical Engineering, Far East University, Tainan, Taiwan.

with the interface between the solder and the region with dissolved Ag [3]. A nickel film is often electroplated onto the silver conductor surface to serve as a soldering barrier to prevent silver leaching. However, metal electroplating is unsuitable for semi-conductive ceramic components because it complicates production [4]. Solder leaching can also be reduced by using a conductor paste based on a mixed metal powder of Ag and palladium (Pd) or platinum (Pt) instead of a paste made of only Ag [5]. However, the addition of Pd or Pt into silver paste increases resistivity, leading to higher conductor loss. Moreover, Pd and Pt are more expensive than Ag and thus increase production costs. Therefore, it is crucial to improve the solderability between silver conductors and lead-free solder without using expensive precious metals or Ni electroplating to produce electronic components.

Related studies have mainly focused on the addition of oxides, such as SiO_2 [6], Al_2O_3 [7], and ZrO_2 [8], to lead-free solder to inhibit the growth of IMCs and hence promote the solderability between silver conductors and lead-free solder. However, the effects of these oxides on solderability and resistance to silver leaching are not fully known [1]. In this study, oxides were added into the silver paste to improve resistance to silver leaching, and the growth mechanism of an IMC between a silver conductor and lead-free solder was investigated.

2 Experimental procedure

2.1 Sample preparation

A commercial silver powder (D_{50} = 1.9 µm) purchased from Ample Electronic Co. Ltd. was used as the raw material. Figure 1 shows the scanning electron microscopy (SEM) morphology of the silver powder. As shown, the silver particles are spherical. Tetraethyl orthosilicate (TEOS, Aldrich) (95%) and ethanol (99.5%) were used for silica deposition, and dimethylamine (DMA, Aldrich) (50%) was used as the catalyst for a sol–gel reaction of TEOS. Amorphous silica was deposited onto the surface of the silver powder through hydrolysis and a condensation reaction of TEOS based on the Stöber method [9]. TEOS, a silica precursor, was first hydrolyzed for 20 min in a mixture of deionized water and ethanol in the presence of DMA as a catalyst. The Stöber reactant compositions are shown in Table 1. During the condensation reaction, 10 g of silver powder was added into the pre-hydrolysis TEOS solution. The reaction was maintained at 30 °C for 10, 24, and 48 h, and the particles were washed with deionized water and collected by centrifugation at 4000 rpm for 5 min to obtain the silica-deposited silver powder. The silver paste was prepared by premixing the silver powder with an organic vehicle (ethyl cellulose solution) purchased from Ample Electronic Co. Ltd. using a planetary centrifugal mixer (the ratio of silver powder to the organic vehicle was 70:30) [10]. The paste was then passed through a zirconia triple-roller mill to break the agglomerates. This process was repeated several times to obtain a homogeneous paste with a degree of fineness of under 10 µm. The flowchart for the silver paste preparation is shown in Fig. 2. The silver paste was screen-printed onto an alumina substrate and fired at 850 °C for 15 min. Sn3.0Ag0.5Cu solder pastes (Senju Metal Industry Co., Ltd.) were then screen-printed onto the silver conductor with the size of 3 × 3 mm and thickness of about 150 µm, undergoing a reflow process with peak temperatures of 240 °C, 260 °C, 280 °C, and 300 °C for various durations.

Fig. 1 SEM morphology of silver powders

2.2 Characterization

Field-emission transmission electron microscopy (FE-TEM, JEOL JEM-2100F) was used to observe the IMC and silica nanoparticle (NP) morphology. The microstructure was observed using SEM (Hitachi, S4100, Tokyo, Japan), and the distribution of elements was measured using electron probe microanalysis (EPMA) (JEOL, JXA-8900R, Tokyo, Japan). The silica-deposited silver powders were characterized using Fourier transform infrared spectroscopy (FTIR, EQUINO 55, Brucker). FTIR spectra were obtained using the

Table 1 Stöber reactant compositions

Sample	TEOS (g)	DMA (ml)	H_2O (ml)	EtOH (ml)	DMA (ml)
1 wt% TEOS	0.1	1	20	79	1
3 wt% TEOS	0.3	2	20	78	2
5 wt% TEOS	0.5	3	20	77	3

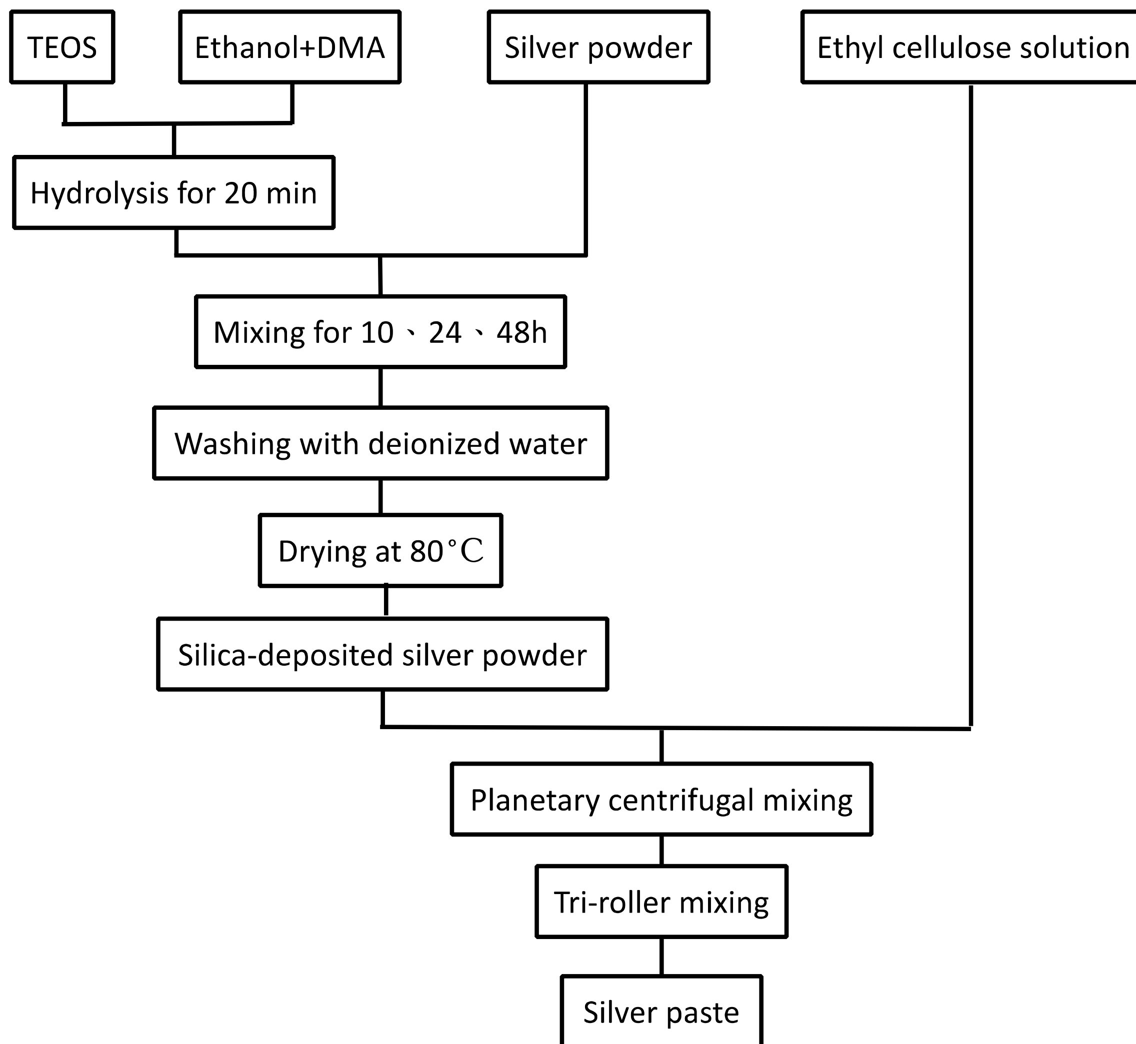

Fig. 2 Flowchart for the silver paste preparation

KBr pellet technique (sample/KBr = 1/100). The crystalline phase identification was determined using X-ray diffractometry (Dandong Fangyuan, DX-2700, Sandong, China) with CuK*α* radiation.

3 Results and discussion

Figure 3 shows SEM images of silver powders coated with various amounts of TEOS for different reaction times. Table 2 offers the SiO_2 content of these silver powders determined using energy-dispersive X-ray spectroscopy (EDS). The amount of silica NPs coated onto the silver powder surface increased with increasing reaction time and TEOS addition. For samples with 5 wt% TEOS addition and a reaction time of 48 h, the silica NPs covered almost the entire silver powder. These conditions resulted in the highest silica coating content. For the sample with 1 wt% TEOS addition, the silica NPs coating was inhomogeneous (higher square deviation in Table 2), and much of the silver powder surface was uncovered even after a reaction time of 48 h.

Figure 4 shows the FTIR spectra of silver powders coated with various amounts of TEOS and a reaction of 48 h. The FTIR peaks at 470, 1086, 1410, 1630, 1710, and 3000–3600 cm^{-1} are attributed to the bending and stretching of Si–O–Si, C–H vibration, Si–OH vibration, C–O stretching, and O–H vibration of the adsorbed water, respectively [11–13]. These results confirm that the NPs coated onto the silver powder surface were SiO_2. The characteristic absorption peak intensity of Si–O–Si increases with increasing reaction time, which is consistent with the SEM results.

Figure S1 shows cross-sectional SEM images of the interfaces after soldering at 240–300 °C for various times for silver pastes without TEOS. After soldering for 15 s at 240 °C, thin Ag_3Sn intermetallic layers with

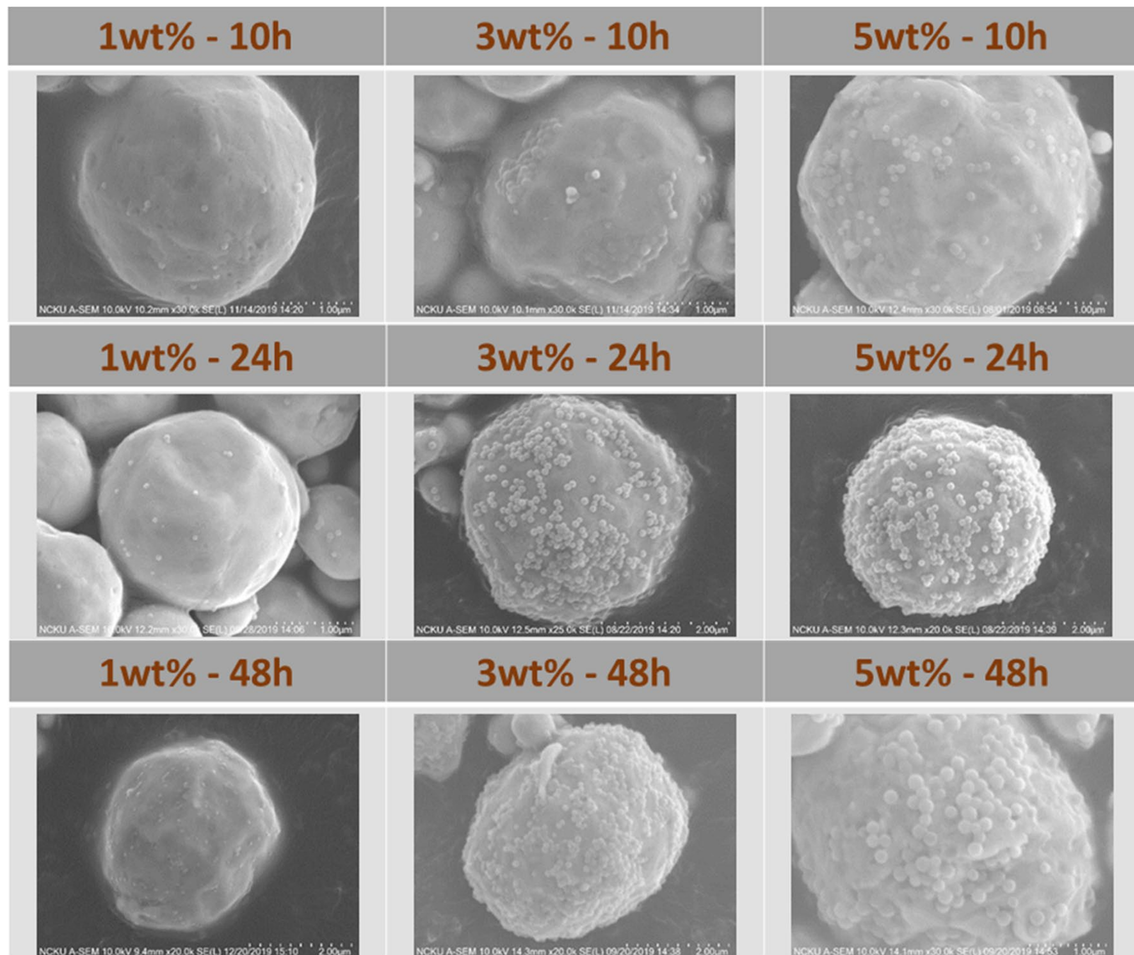

Fig. 3 SEM images of silver powders coated with various amounts of TEOS for various reaction times

Table 2 SiO_2 content for silver powders after coating with various amounts of TEOS (results based on EDS)

TEOS addition	SiO_2 content (wt%)		
	Reaction time		
	10 h	24 h	48 h
1 wt%	0.2 ± 0.1	0.36 ± 0.15	0.6 ± 0.47
3 wt%	0.56 ± 0.21	0.78 ± 0.26	0.92 ± 0.14
5 wt%	0.65 ± 0.5	0.85 ± 0.5	1.3 ± 0.25

an average thickness of 18 μm appeared, and shallow grooves formed at the Ag_3Sn grain boundaries. After 60 s at 240–280 °C, the grooves deepened towards the Ag conductor and made contact with the alumina substrate due to IMC dissolution at Ag_3Sn grain boundaries during the soldering (i.e., silver leaching). At a soldering temperature of 300 °C, silver leaching occurred within 15 s. These results suggest that the silver paste without a SiO_2 coating cannot withstand high-temperature soldering.

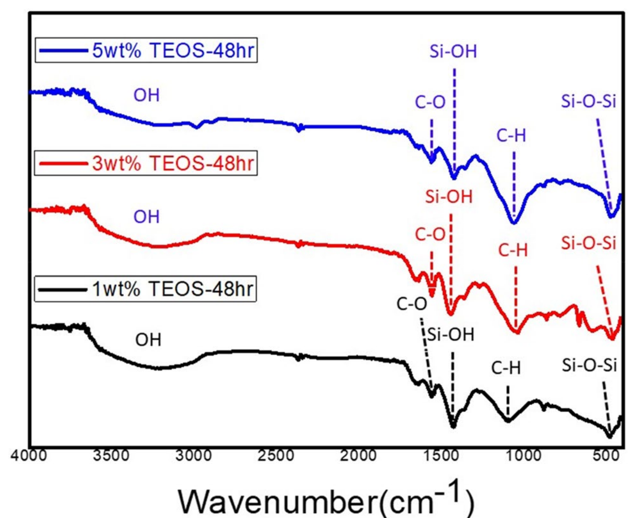

Fig. 4 FTIR spectra of silver powders coated with various amounts of TEOS for a reaction time of 48 h

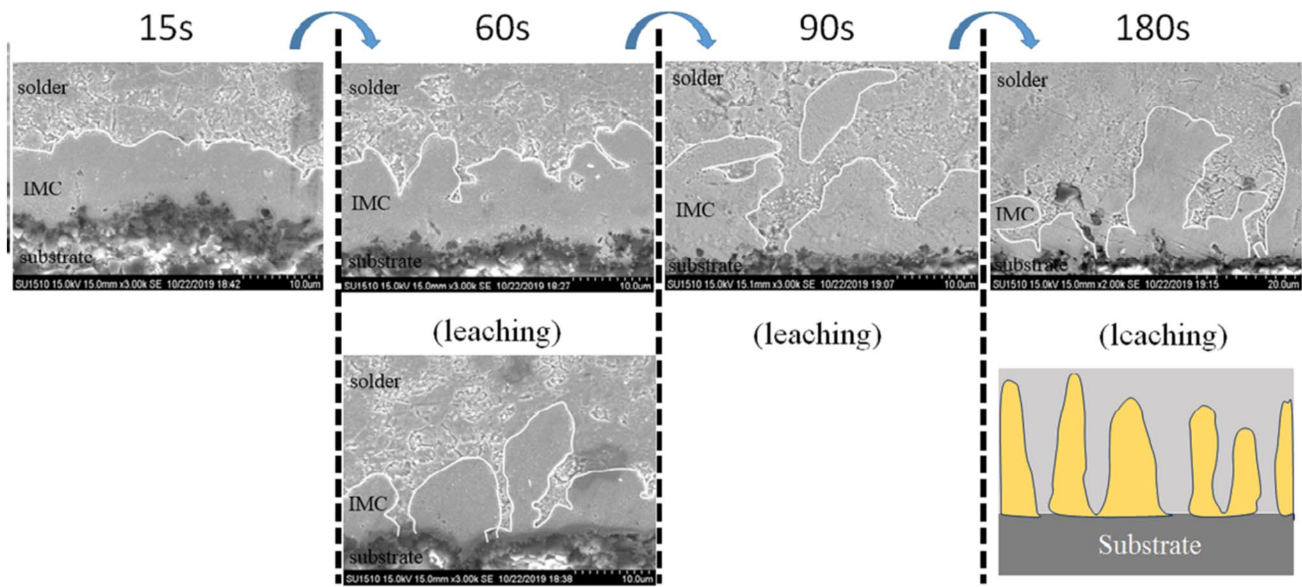

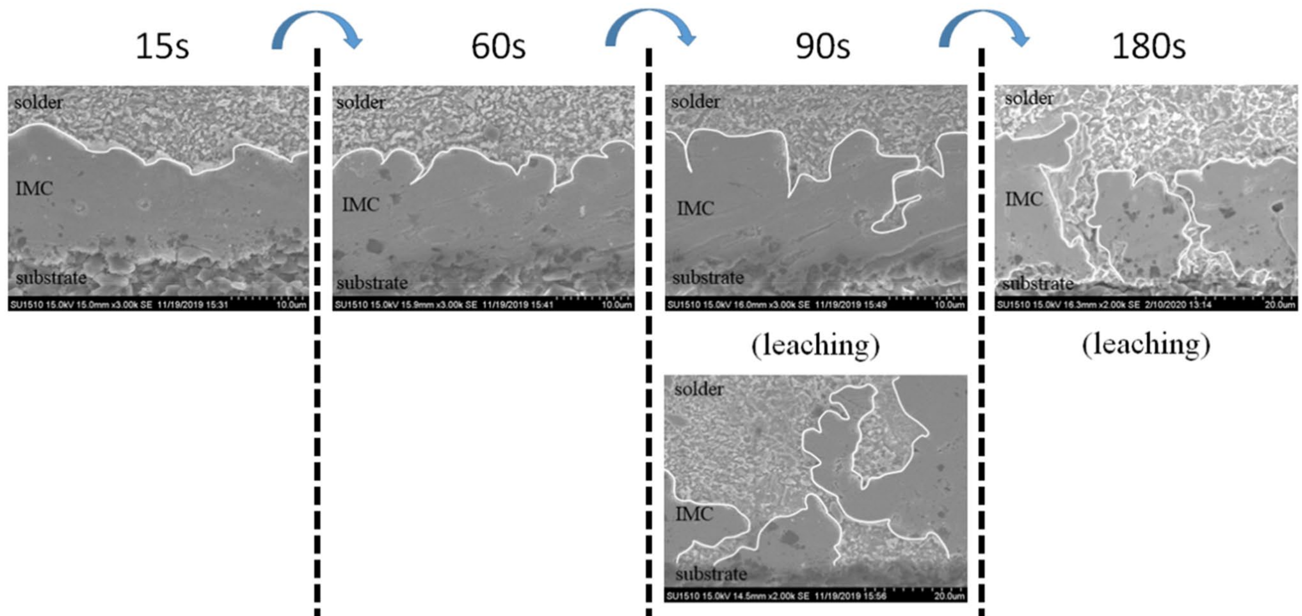

Fig. 5 Cross-sectional SEM images of interfaces after soldering at 260 °C and 280 °C for various times for silver pastes with 1 wt% TEOS at reaction times of 10 and 48 h

Figures 5 and 6 show cross-sectional SEM images of the interfaces after soldering at 260 °C and 280 °C for various times for silver pastes with 1 wt% and 5 wt% TEOS at reaction times of 10 and 48 h, respectively. The grooves deepened towards the Ag conductor as the soldering temperature increased, shortening the silver leaching time. For the sample coated with 1 wt% TEOS after a reaction for 10 h, silver leaching was observed after

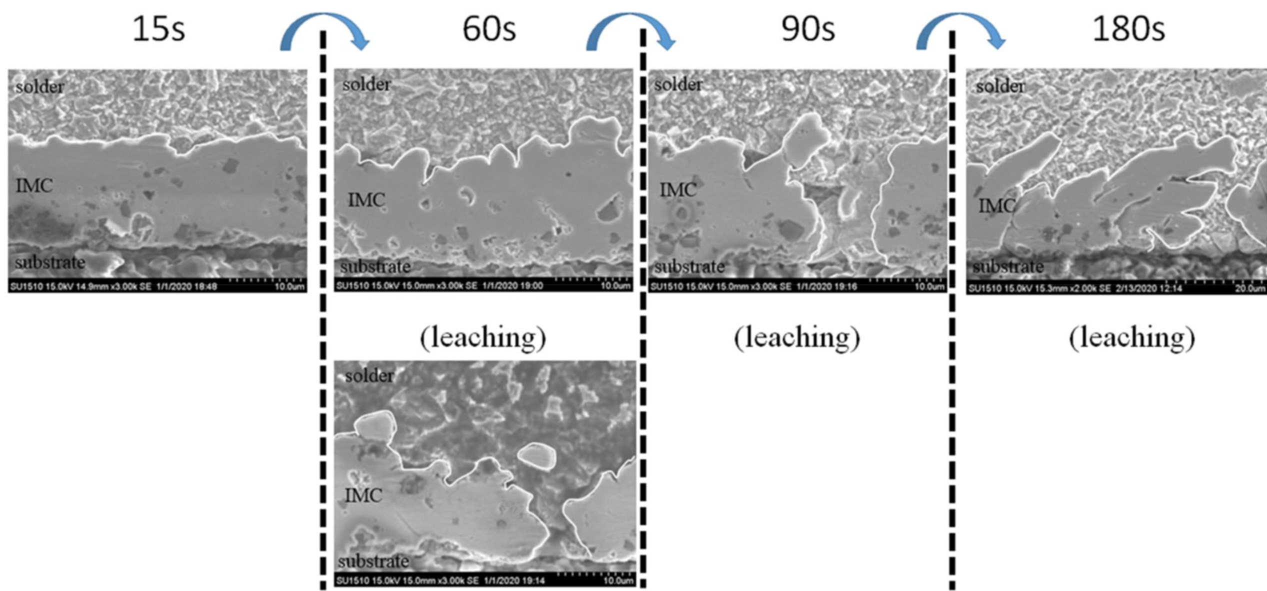

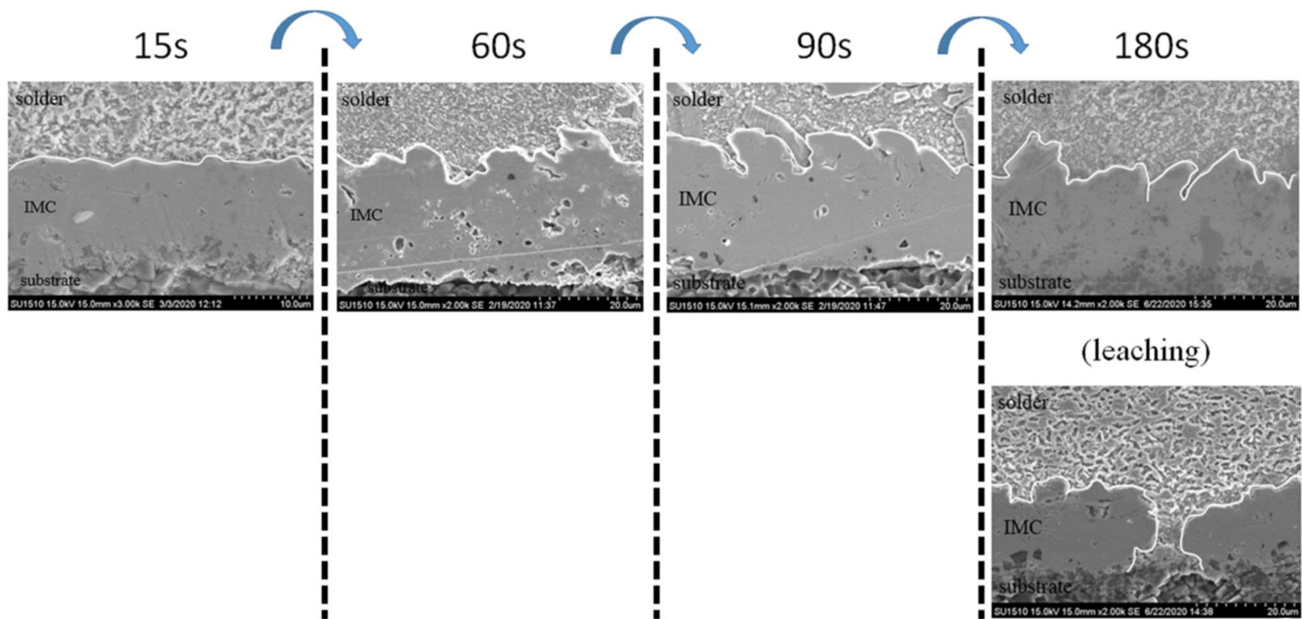

Fig. 6 Cross-sectional SEM images of interfaces after soldering at 260 °C and 280 °C for various times for silver pastes with 5 wt% TEOS at reaction times of 10 and 48 h

soldering at 260 °C for 60 s. When the reaction was prolonged to 48 h, the silver leaching time was extended to above 180 s and 90 s at soldering temperatures of 260 °C and 280 °C, respectively. In contrast, for the sample coated with 5 wt% TEOS after a reaction for 48 h, silver leaching did not appear until 180 s after soldering at

280 °C. These results suggest that coating SiO_2 onto a silver powder surface can effectively retard silver leaching.

Figure 7 shows focused ion beam (FIB) and TEM images of the soldered sample coated with 5 wt% TEOS after a reaction for 48 h. The two regions shown in Fig. 7a were

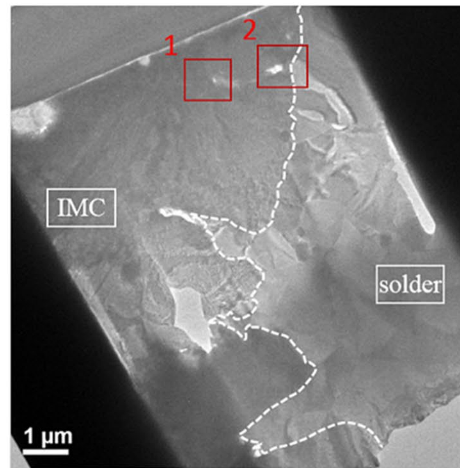

(a)

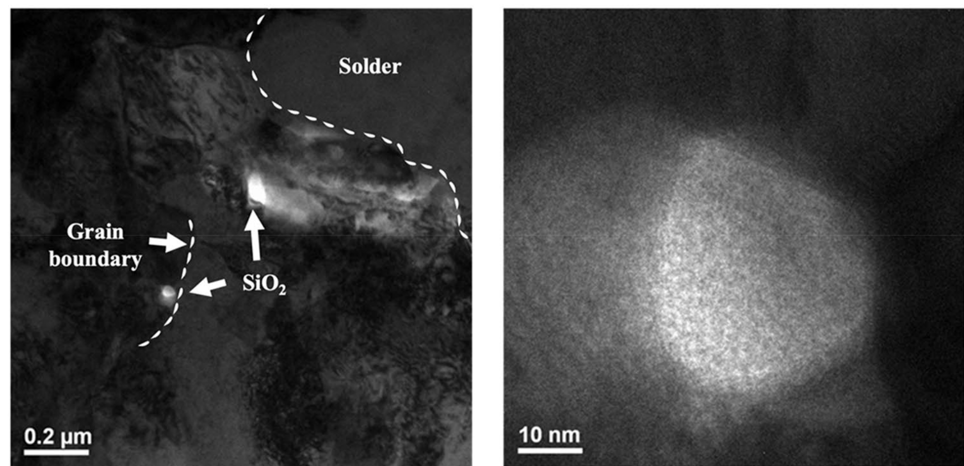

(b)

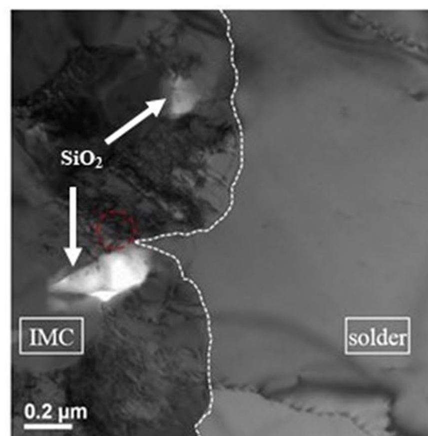

(c)

Fig. 7 (a) FIB and TEM images in (b) region 1 and (c) region 2 for soldered sample coated with 5 wt% TEOS for a reaction time of 48 h

investigated. In region 1, SiO_2 NPs appeared at the IMC grain boundaries. The silica NPs were amorphous, as determined from high-resolution TEM images (Fig. 7b). In region 2, silica NPs appeared at the grain boundary close to the tip of the shallow groove (Fig. 7c). It is believed that the formation of the groove is due to IMC dissolution at Ag_3Sn grain boundaries; the IMC at grain boundaries continually dissolved into the molten solder, deepening the grooves and inducing silver leaching [14, 15]. The silica NPs located at grain boundaries can hinder the dissolution of the IMC by the molten solder along grain boundaries and hence retard silver leaching.

A schematic diagram of the proposed IMC formation for the silver paste coated with silica NPs is shown in Fig. 8. Tang et al. [16] investigated the effects of adding CeO_2 nanoparticles on the formation and growth of IMCs between Sn-0.3Ag-0.7Cu-$x$$CeO_2$ solders and Cu substrates during reflow soldering. Zhang et al. [17] studied the effects of adding La_2O_3 nanoparticles into Sn3.8Ag0.7Cu solder on the interfacial microstructures of the SnAgCu/Cu solder joints. They both observed that some oxide nanoparticles became heterogeneous nucleation sites for Cu-Sn phases. When the Ag conductor contacts with molten solder, silica NPs may serve as heterogeneous nucleation centers for the nucleation of Ag_3Sn (IMC) (Step I). Once a stable IMC layer forms, the silica NPs are located at the IMC grain boundaries (Step II). As the soldering temperature or time increases, the IMC is dissolved by the molten solder along grain boundaries during soldering, resulting in the formation of a groove. Silica NPs can hinder the dissolution of the IMC by the molten solder along grain boundaries during soldering, retarding silver leaching (Step III).

The relationship between the IMC thickness and soldering time can be expressed as [18–20]:

$$H = kt^n \quad (1)$$

where H is the IMC thickness, k is the growth rate, t is the soldering time, and n is the time exponent, representing the diffusion mechanism. When n is < 0.5, the growth mechanism of the interface IMC is dominated by bulk diffusion. When n is between 0.5 and 1, the growth mechanism of the interface IMC is controlled by grain boundary diffusion [16].

The plots of log H versus log$t$ for samples after a reaction for 24 and 48 h are shown in Fig. 9. There were not enough IMC thickness data for the samples coated with TEOS after a reaction for 10 h because silver leaching appeared earlier. The slope representing the time exponent (n) and the goodness-of-fit are summarized in Tables 3 and 4. The result shows that the time exponent n for all samples is less than 0.5, indicating that the growth mechanism of the IMC is mainly controlled by bulk diffusion. The n value decreased with increasing TEOS addition or reaction time, suggesting that grain boundary diffusion was effectively inhibited by the silica NPs located at IMC grain boundaries.

Tables 5 and 6 show the growth rate k for samples coated with TEOS after soldering at various

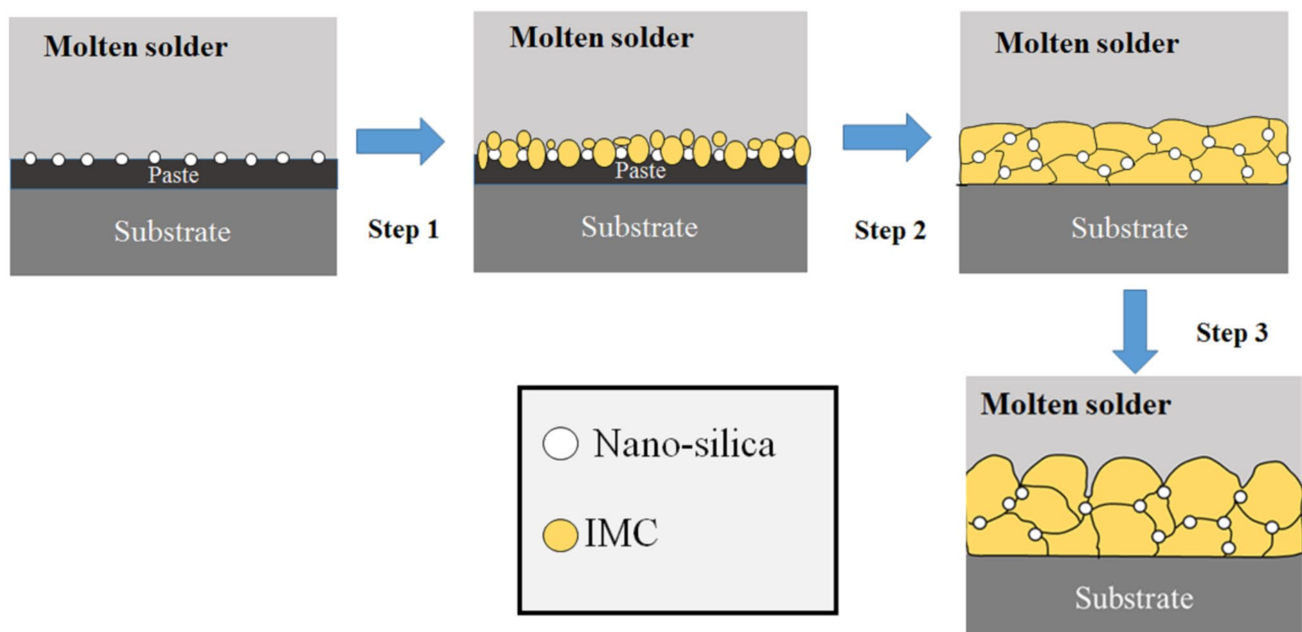

Fig. 8 Schematic diagram of proposed IMC formation for silver paste coated with silica NPs

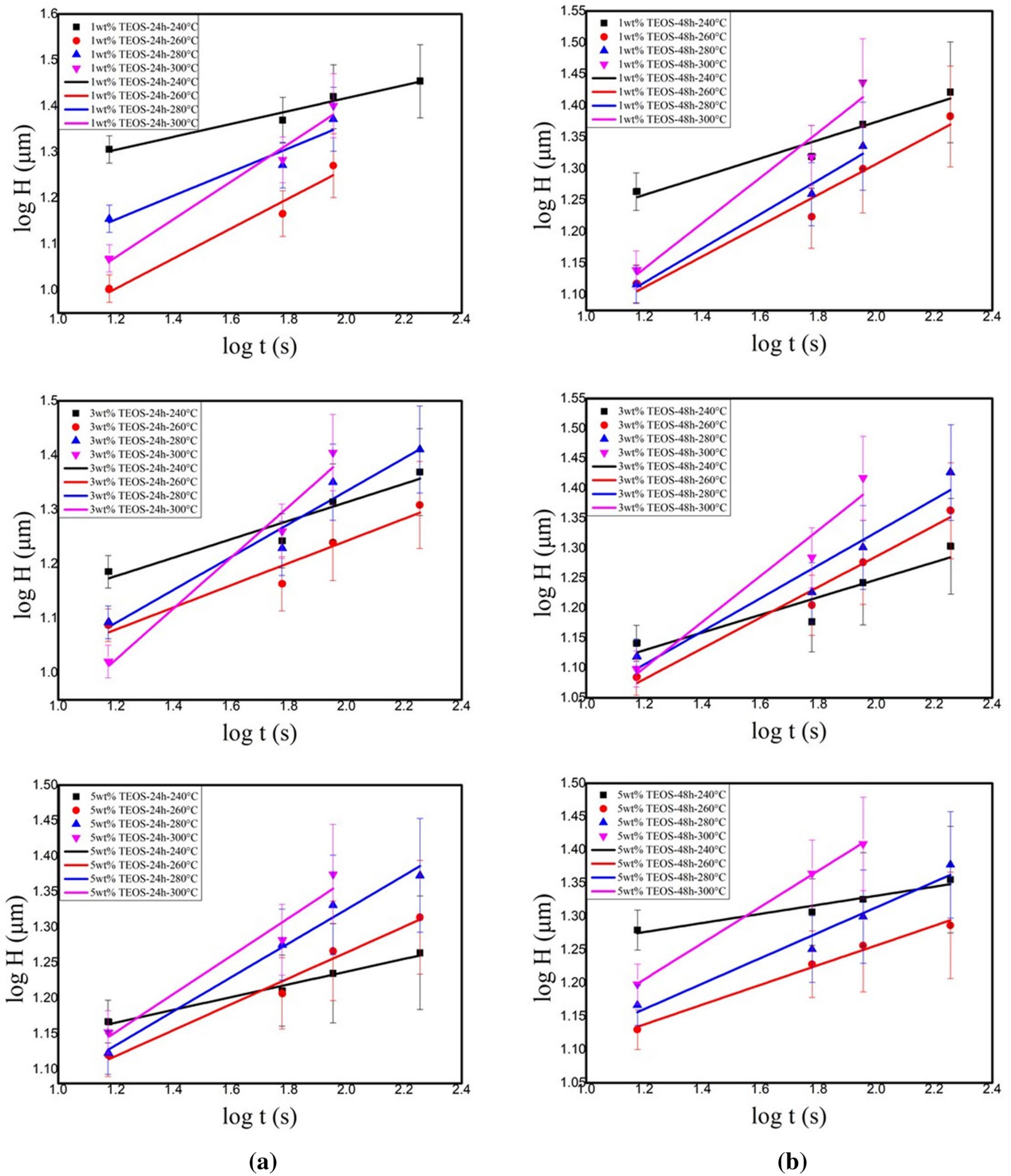

Fig. 9 Plots of log H versus logt for samples after reaction for (a) 24 h and (b) 48 h

Table 3 Time exponent (n) and the goodness-of-fit (R^2) for samples coated with TEOS and reacted for 24 h after soldering at various temperatures

Soldering temperature	1 wt% TEOS		3 wt% TEOS		5 wt% TEOS	
	n	R^2	n	R^2	n	R^2
240 °C	0.14	0.95	0.17	0.89	0.09	0.98
260 °C	0.32	0.94	0.20	0.92	0.18	0.97
280 °C	0.25	0.87	0.30	0.94	0.24	0.98
300 °C	0.41	0.96	0.47	0.95	0.27	0.91

Table 4 Time exponent (n) and the goodness-of-fit (R^2) for samples coated with TEOS and reacted for 48 h after soldering at various temperatures

Soldering temperature	1 wt% TEOS		3 wt% TEOS		5 wt% TEOS	
	n	R^2	n	R^2	n	R^2
240 °C	0.14	0.92	0.15	0.81	0.07	0.92
260 °C	0.24	0.95	0.26	0.97	0.15	0.98
280 °C	0.27	0.97	0.28	0.91	0.19	0.95
300 °C	0.36	0.93	0.38	0.91	0.27	0.99

Table 5 Growth rate for samples coated with TEOS and reacted for 24 h and after soldering at various temperatures

Soldering temperature	Growth rate ($\times 10^{-12}$) m^2/s		
	1 wt% TEOS	3 wt% TEOS	5 wt% TEOS
240 °C	0.797	0.764	0.151
260 °C	2.178	0.767	0.633
280 °C	2.520	2.118	1.195
300 °C	5.424	6.489	2.625

Table 6 Growth rate for samples coated with TEOS and reacted for 48 h after soldering at various temperatures

Soldering temperature	Growth rate ($\times 10^{-12}$) m^2/s		
	1 wt% TEOS	3 wt% TEOS	5 wt% TEOS
240 °C	0.747	0.464	0.147
260 °C	1.397	1.346	0.376
280 °C	2.245	2.061	0.939
300 °C	5.365	5.318	3.165

temperatures. As the amount of TEOS and reaction time increased, the growth rate of the IMC decreased. The interfacial IMC growth activation energy can be obtained from the Arrhenius equation [18–20]:

$$k = k_0 \exp\left(-\frac{Q}{RT}\right) \tag{2}$$

where k is the growth rate, k_0 is the growth constant, Q is the activation energy, R is the ideal gas constant, and T is the temperature. The plots of ln k versus ln t for samples

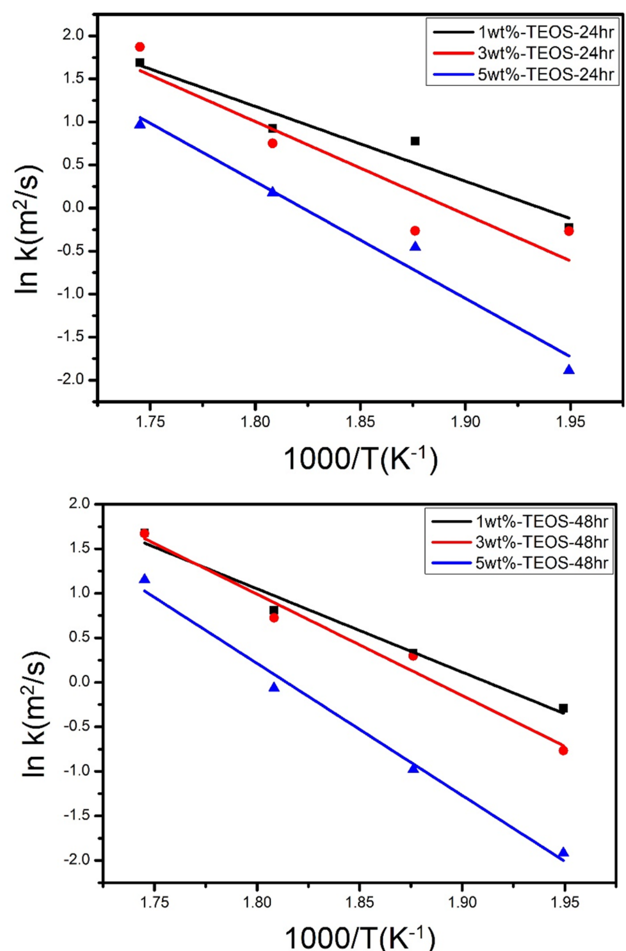

Fig. 10 Plots of ln k versus 1/T for samples after reaction for 24 and 48 h

Table 7 Activation energies of interfacial IMC growth for samples coated with TEOS and reacted for 24 h and 48 h after soldering

Reaction time	Activation energy (kJ/mol)		
	1 wt% TEOS	3 wt% TEOS	5 wt% TEOS
24 h	72	89	112
48 h	77	95	123

after a reaction for 24 and 48 h are shown in Fig. 10. The activation energies of the interfacial IMC growth for the samples coated with TEOS after soldering are listed in Table 7. The growth activation energy increased with increasing TEOS addition and reaction time. This result confirms that the TEOS coating slows interfacial IMC growth during soldering. This can be explained by the fact that silica NPs inhibit the silver diffusion.

4 Conclusion

(1) Silica NPs were coated onto the surface of silver powders through hydrolysis and a condensation reaction of TEOS based on the Stöber method.
(2) Silica NPs located at the IMC (Ag_3Sn) grain boundaries effectively hinder IMC dissolution by molten solder along grain boundaries during soldering, and hence retard silver leaching.
(3) The growth of the IMC is mainly dominated by bulk diffusion for samples coated with TEOS. The growth activation energy increased with increasing TEOS addition and reaction time.

Acknowledgements The research was partially supported by the Ministry of Science and Technology, Taiwan (109-3111-8-006-001) and Ample Electronic Co. Ltd., Taiwan.

Declarations

Conflict of interest No conflict of interest exits in the submission of this manuscript.

Open Access This article is licensed under a Creative Commons Attribution 4.0 International License, which permits use, sharing, adaptation, distribution and reproduction in any medium or format, as long as you give appropriate credit to the original author(s) and the source, provide a link to the Creative Commons licence, and indicate if changes were made. The images or other third party material in this article are included in the article's Creative Commons licence, unless indicated otherwise in a credit line to the material. If material is not included in the article's Creative Commons licence and your intended use is not permitted by statutory regulation or exceeds the permitted use, you will need to obtain permission directly from the copyright holder. To view a copy of this licence, visit http://creativecommons.org/licenses/by/4.0/.References

1. Nakayama K, Nagai A, Iida N (2007) Pb-free silver conductive paste with high reliability. Mater Trans 48:594–599
2. Kattner UR (2002) Phase diagrams for lead-free solder alloys. JOM 54:45–51
3. Zou H, Zhu Q, Zhang Z (2008) Growth kinetics of intermetallic compounds and tensile properties of Sn–Ag–Cu/Ag single crystal joint. J Alloys Compd 461:410–417
4. Hsiang HI, Mei LT, Lin YH (2009) Formation and growth of manganese phosphate passivation layers for NTC ceramics. J Alloys Compd 484:723–728
5. Takeda Y (1994) Basics of electronic packaging technology. Society of Hybrid Microelectronics, pp 53–61
6. Wang Y, Zhao X, Xie X, Gu Y, Liu Y (2015) Effects of nano-SiO 2 particles addition on the microstructure, wettability, joint shear force and the interfacial IMC growth of Sn3. 0Ag0. 5Cu solder. J Mater Sci Mater Electron 26:9387–9395
7. Chuang TH, Wu MW, Chang SY, Ping SF, Tsao LC (2011) Strengthening mechanism of nano-Al 2 O 3 particles reinforced Sn3. 5Ag0. 5Cu lead-free solder. J Mater Sci Mater Electron 22:1021–1027
8. Shen J, Liu YC, Han YJ, Tian YM, Gao HX (2006) Strengthening effects of ZrO 2 nanoparticles on the microstructure and microhardness of Sn-3.5 Ag lead-free solder. J Electron Mater 35:1672–1679
9. Kobayashi Y, Katakami H, Mine E, Nagao D, Konno M, Liz-Marzán LM (2005) Silica coating of silver nanoparticles using a modified Stöber method. J Colloid Interface Sci 283:392–396
10. Hsiang HI, Fan LF, Cheng HY (2015) Silver end termination paste preparation for chip inductor applications. J Alloys Compd 650:835–843
11. Sun SY, Ge YY, Tian ZB, Zhang J, Xie ZP (2017) A simple method to ameliorate hierarchical porous structures of SiO2 xerogels through adjusting water contents. Adv Powder Tech 28:2496–2502
12. Rubio F, Rubio J, Oteo J (1998) FT-IR study of the hydrolysis of tetraethylorthosilicate (TEOS). Spectrosc Lett 31:199–219
13. Dubey R, Rajesh Y, More M (2015) Synthesis and characterization of SiO2 nanoparticles via sol-gel method for industrial applications. Mater Today-Proc 2:3575–3579
14. Shao H, Wu A, Bao Y, Zhao Y, Liu L, Zou G (2017) Interactions at the planar Ag3Sn/liquid Sn interface under ultrasonic irradiation. Ultrason Sonochem 39:758–764
15. Li JF, Agyakwa PA, Johnson CM (2010) Kinetics of Ag3Sn growth in Ag–Sn–Ag system during transient liquid phase soldering process. Acta Mater 58:3429–3443
16. Tang Y, Guo QW, Luo SM, Li ZH, Li GY, Hou CJ, Zhong ZY, Zhuang JJ (2019) Formation and growth of interfacial intermetallics in Sn-0.3 Ag-0.7 Cu-xCeO2/Cu solder joints during the reflow process. J Alloys Compd 778:741–755
17. Zhang L, Gao L (2015) Interfacial compounds growth of SnAgCu (nano La2O3)/Cu solder joints based on experiments and FEM. J Alloys Compd 635:55–60
18. Bai H, Long Z, Chen J, Gu X, Lv J, Zhao L, Chen D, Yan J (2010) J Mater Sci Mater Electron 31:10105–10112
19. Yoon JW, Lee CB, Jung SB (2002) Interfacial reactions between Sn-58 mass% Bi eutectic solder and (Cu, electroless Ni-P/Cu) substrate. Mater Trans 43:1821–1826
20. Yoon JW, Jung SB (2003) Investigation of interfacial reactions between Sn–5Bi solder and Cu substrate. J Alloys Compd 359:202–208

Publisher's Note Springer Nature remains neutral with regard to jurisdictional claims in published maps and institutional affiliations.